# Microwave Detection of Breast Cancer

E. C. Fear, *Student Member, IEEE,* and M. A. Stuchly, *Fellow, IEEE*

***Abstract*—Breast cancer affects many women, and early detection aids in fast and effective treatment. Mammography, which is currently the most popular method of breast screening, has some limitations, and microwave imaging offers an attractive alternative. A microwave system for breast tumor detection that uses previously introduced confocal microwave imaging techniques is presented in this paper. The breast is illuminated with an ultrawide-band pulse and a synthetic scan of the focal point is used to detect tumors; however, the geometric configuration and algorithms are different from those previously used. The feasibility of using small antennas for tumor detection is investigated. Signal processing algorithms developed to mitigate the dominant reflection from the skin are described, and the effectiveness of these skin subtraction algorithms is demonstrated. Images of homogeneous and heterogeneous breast models are reconstructed with various numbers of antennas. Both the influence of antenna spacing and the suitability of simplified models for system evaluation are examined.**

***Index Terms*—Microwave imaging, tumor detection, ultrawide-band antennas.**

## I. Introduction

MICROWAVE imaging of biological structures has been of interest for many years. Recently, microwave imaging has been applied to the detection of breast cancer [1]–[3]. This approach appears promising due to the accessibility of the breast for imaging and the high contrast between normal breast tissue and tumors. Early work in the area of microwave imaging is summarized in [4]. With developments in image reconstruction algorithms, computational methods, and increased computing power, advances in microwave imaging have been realized. These solutions generally involve measurement of energy transmitted through an object placed in a water or saline bath. The measurements are then used to reconstruct the material properties of the object. For example, the chirp computed tomography (CT) system developed by Miyakawa *et al.* isolates the signal traveling directly from transmitting to receiving antennas, using the frequency component of the beat signal corresponding to the distance between the antennas [5]. This allows for application of X-ray CT reconstruction algorithms. Another approach to reconstructing the object profile solves the inverse scattering problem using iterative methods. This involves computation of received energy with a numerical method and an estimate of material properties (the forward problem), and application of optimization to determine corrections in material properties for a better match between the measured and computed data. In conjunction with these approaches, prototype systems have been introduced. Paulsen *et al.*have developed a system that operates between 500–900 MHz, and consists of an array of monopole antennas [1], [6]. The hybrid finite-element boundary-element method is used to solve the forward problem, and then the Newton–Raphson iterative method is applied to solve the inverse-scattering problem. To correct for coupling between array elements, a nonactive antenna compensation model that is obtained empirically is incorporated into the reconstruction. This model produces well-localized images of real and imaginary parts of the wavenumber. Franchois *et al.*have developed a 2.45-GHz microwave camera, which consists of transmitting and receiving horns, with an array of 32 $\times$ 32 small dipoles positioned in the receiving horn [7]. The method of moments combined with the distorted Born iterative approach is used in image reconstruction. Another system developed by Souvorov *et al.* consists of an object placed in a water bath and surrounded by 32 transceivers operating at 2.45 GHz [8]. Measurements are made at the 16 antennas located across from the excited antenna. To reconstruct images, a fast iterative method is used for the direct solution, and the Newton iterative method is applied to the inverse solution. Chew has developed a time-domain approach that incorporates the finite-difference time-domain (FDTD) method in the distorted-Born iterative method to reconstruct images [9]. This has been combined with time-domain impulse radar to produce a system for nondestructive testing, and has the added the advantage of information for target recognition available from ultrawide-band illumination [10]. In terms of application to the breast imaging problem, the system proposed by Meaney *et al.* [1] has been used to image excised breast tissue with and without inclusions of saline "tumors." The promising initial results indicate that this is a feasible approach to breast cancer detection.

Our approach to breast cancer detection differs from traditional microwave imaging, as it involves identification of regions of increased scatter as opposed to directly imaging tissue electrical properties. Our method is similar to that of Hagness *et al.* [2], [3], and was introduced in [11]. The breast is illuminated with an ultrawide-band pulse, and the backscattered signal is recorded. This is repeated for a number of antenna positions. A time-shift-and-add algorithm is applied to the set of recorded signals in order to enhance returns from high-contrast objects and reduce clutter. This involves computing the time delay for the roundtrip between each antenna to a point in the domain of interest, then adding the corresponding portions of the time signals recorded at each antenna. The same image-formation process is used in several synthetic aperture ground penetrating radar systems, which detect, for example, unexploded buried ordinances and steel reinforcement beams in roads and bridges [12], [13]. These synthetic aperture radars are wide-band, thus,

Manuscript received November 18, 1999; revised January 25, 2000. This work was supported by the National Sciences and Engineering Research Council of Canada.

The authors are with the Department of Electrical and Computer Engineering, University of Victoria, Victoria, BC, Canada V8W 3P6 (e-mail: efear@engr.uvic.ca).

Publisher Item Identifier S 0018-9480(00)09536-3.

time shifting is used instead of the phase correction incorporated into the narrow-band version. The ultrawide-band signal provides high resolution, as resolution is inversely proportional to bandwidth. The creation of images does not involve complex reconstruction algorithms, however, there is a tradeoff between simplicity and information obtained, as material properties are not recovered, as in microwave imaging. Additional information extracted from the raw ultrawide-band signals may be used to gain further insight into the detected object.

The application of ground penetrating radar ideas to breast cancer detection was introduced by Hagness *et al.* [2],[3]. Their initial two-dimensional (2-D) simulations showed feasibility of detecting tumors in a heterogeneous background, including the presence of other structures such as veins and random perturbations of tissue properties. The technique was also found to be robust to the presence of material dispersion. The breast was illuminated with an ultrawide-band signal by an antenna placed on the breast. The upper frequency was limited to about 10 GHz to maintain reasonable attenuation. Further three-dimensional (3-D) simulations investigated the performance of a resistively loaded bowtie antenna element for this sensing application, indicating the possibility of detecting spherical tumors on the order of 2-mm diameter at 5-cm depth. Use of spectral signatures related to tumor shape and cross-polarization to distinguish tumors in, for example, returns from the chest wall were also examined.

We have further explored adaptation of the ground penetrating radar ideas to breast cancer detection. The alternative physical configuration of our proposed system involves encircling the breast, which is immersed in a low-loss material similar to either breast tissue or skin, with an array of antennas. As the volume inside of the array is imaged, this provides a frame of reference for the image reconstruction. Since the antennas are placed at a distance from the skin, new image reconstruction algorithms are required to reduce the dominant reflection from the skin. Additionally, we test the feasibility of using smaller antennas, which are less sensitive than previously investigated bow ties, for tumor detection. Section II describes the system configuration and models. In Section III, the simulation methods and image reconstruction algorithms are outlined. Results are presented in Section IV, and include antenna characterization, the effectiveness of the skin subtraction algorithm, and a comparison of images with various approaches to detection. The algorithms are developed for the system immersed in low-loss breast tissue; however, antenna characterization and initial feasibility studies of the system immersed in low-loss skin are included. A discussion of the results is provided in Section V, and brief conclusions are presented in Section VI.

## II. Models

### A. System Configuration

A representation of one plane of the proposed system is shown in Fig. 1. The patient lies in a prone position with the breasts immersed in a liquid with electrical properties similar to those of breast tissue or skin, but of low loss. An array of antennas is placed in the liquid, and positioned in a circle around and offset from the breast. For data acquisition, one antenna transmits an ultrawide-band pulse and the scattered returns are recorded at the same antenna. This is repeated sequentially for each antenna in the array. The antennas are spaced to reduce their coupling; however, the array may be rotated to a new position for acquisition of additional data. Furthermore, translating the array vertically allows for scans of different cross sections through the breast.

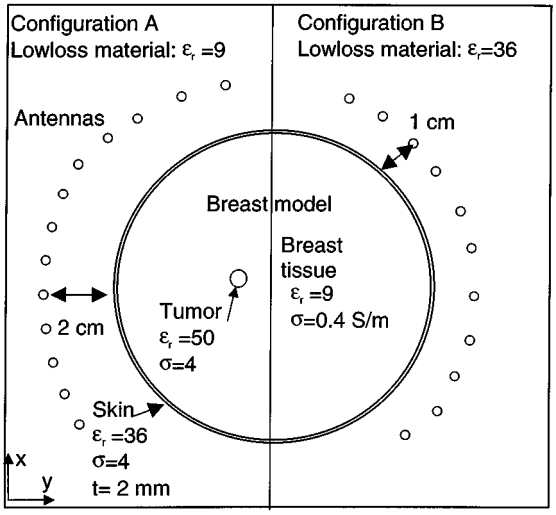


Fig. 1. System configuration. Configuration A is immersed in a low-loss breast-like substance and the distance from antenna to object is 2 cm. Configuration B is immersed in a low-loss skin-like substance and the distance from antenna to object is 1 cm.

This antenna configuration provides a frame of reference for image reconstruction. That is, the location of the antennas is known, and the volume inside of the array of antennas is scanned without significant *a priori* information about the position of the breast. In the previous configuration [2], [3], the antennas are positioned on the surface of the breast and the physical locations of the antennas must be determined for input into the image reconstruction algorithms. On the other hand, the circular array does not provide the ability to scan the upper outer quadrant of the breast where many tumors occur. Further modifications to the antenna arrangement may alleviate this limitation. Additionally, the reflection from the skin is the most significant of the returns recorded by antennas located at a distance from the breast. This may overwhelm responses from small tumors in reconstructed images, and must be addressed in image reconstruction algorithms.

### B. Breast Model

The breast is modeled as a finite cylinder of breast tissue surrounded by an outer layer of skin (Fig. 1). This cylindrical model is not realistically shaped, but a reasonable approximation for feasibility studies of tumor detection in 2-D cross sections. The breast models have diameter of 6 cm and length of 7 cm. The diameter of the model is selected as a reasonable cross-sectional dimension of the breast that gives relatively short computational time. In most cases, the skin is modeled as a 2-mm-thick layer. While this thickness may be excessive, it maximizes attenuation of the signals passing through it, providing a robust test of the tumor detection capabilities. The influence of skin thickness

on the reflections from the skin is examined by varying this parameter from 1 to 2.5 mm. Tumors are modeled as spheres of diameters ranging from 2 to 6 mm, and are located at the center of the cylinder at a depth of approximately 3 cm.

The properties of the breast model are similar to those selected by Hagness *et al.* [2]. In most simulations, the breast tissue cylinder is homogeneous and assigned electrical properties of $\varepsilon_r = 9$ and $\sigma = 0.4$ S/m. These values were suggested by Hagness *et al.* [2], and result from extrapolating measurements of normal breast tissue made at lower frequencies to higher frequencies using a Debye model. To consider the influence of natural variations in breast tissue, a heterogeneous cylinder is also simulated. This model consists of 0.4-cm cubes with random perturbations of up to $\pm 10\%$ in the nominal dielectric properties of breast tissue. The skin surrounding the breast tissue cylinder is assigned $\varepsilon_r = 36$ and $\sigma = 4$ S/m. Tumors are modeled as $\varepsilon_r = 50$ and $\sigma = 4$ S/m; the conductivity is less than that of the tumors in [2] and [3]. The entire breast model is immersed in a liquid with the same dielectric constant as either breast tissue or skin, but with very low conductivity. Material dispersion is not incorporated into these models. Hagness *et al.* found dispersion of breast tissue to have a small impact on tumor detection [2]. In the frequency range of interest, skin has small dispersion [14].

### C. Antenna Models

Illumination of breast tissue with a broad-band pulse requires an antenna suited to pulse radiation. The backscattered signal from the tumor must be detected in the presence of clutter, including reflections from the antenna itself. For sensing applications, several antennas have been identified as suitable and most incorporate resistive loading, as this technique has proven effective in reducing reflections from antenna ends. Dipoles and bow ties have better physical compatibility with the problem investigated. This outweighs advantages of improved antenna performance inherent in horns (e.g., directivity). Hagness *et al.*have modified the bow tie for use in biological sensing, obtaining end reflections of less than $-125$ dB [15]. The resistively loaded bow-tie antennas provide excellent sensitivity to reflected signals, however, these antennas are computationally expensive and physically large. Dipoles [16], [17] and vee dipoles [18] with various resistive loading profiles have been previously investigated, showing broad-band behavior with low end reflections and high fidelity. For our preliminary investigations, we selected a simple resistively loaded dipole based on the Wu–King design [19], [20]. These antennas have poor efficiency and directivity, however, they allow for the incorporation of physically small antennas with both reasonable behavior (e.g., bandwidth, fidelity) and computational cost in terms of our system models. These decreased computational costs are the primary reason for selecting dipoles rather than further miniaturizing the bow tie.

To design the Wu–King dipole loading, a frequency in the center of the band ($f_\varphi$) is selected, and the design parameter $\varphi$ is evaluated at this frequency [21], [22]. This method is used to design the loading profiles for two antennas in low-loss breast tissue (antenna 1) and skin (antenna 2). Antenna lengths of $\lambda/2$ in each material are selected to evaluate the feasibility of using small antennas for this application. The antenna model is a rod consisting of short sections. The properties of each section are determined by averaging the Wu–King resistivity profile over the section.

## III. Methods

### A. Antenna Characterization

The antenna element cannot be characterized with traditional frequency-domain measures due to the wide bandwidth over which it operates. Many quantities, such as radiation patterns, usually described in terms of power are better described in terms of energy for wide-band antenna characterization [23]. Far-field distance varies with frequency; however, the far field can be identified by the transition of power variation from $1/R$ to $1/R^2$ [24]. The performance measures for time-domain characterization of antennas used in this paper include frequency-domain transfer functions, and time-domain gain and fidelity [23]–[25]. The transmit transfer function is defined as the ratio of the electric field vector amplitude at a point $P$ to the complex amplitude of the signal at the antenna input [19]. The receive transfer function is the ratio of the complex amplitude response at antenna output port to the source electric-field amplitude at point $P$ in space. Fidelity is defined as [23]

$$F = \max_{\tau} \left[ \int_{-\infty}^{\infty} S(t) E_n(t+\tau)\, dt \right] \tag{1}$$

where $S(t)$ is the normalized signal of interest and $E_n$ is the normalized far-zone radiated electric field. The maximum value of fidelity is one. Time-domain gain is computed as [25]

$$G(\theta, \gamma) = 2\pi r^2 \frac{\displaystyle\int_{-\infty}^{\infty} \frac{|E(\theta, \gamma, t)|^2}{\eta}\, dt}{\displaystyle\int_{-\infty}^{\infty} V_{\text{in}}(t) I_{\text{in}}(t)\, dt} \tag{2}$$

where $V_{\text{in}}$ and $I_{\text{in}}$ are the input voltage and current at the antenna terminals and $E$ is the radiated field. The antenna performance changes with the input signal, as this is inherent in the definition of quantities such as transfer function and fidelity. Transfer functions, fidelity, and time-domain gain require the electric field in the far field. This is assessed by examining the power variation with distance. The effective far-field distance and, therefore, the minimum distance of the breast model from the antenna, is 2 cm in low-loss breast tissue and 1 cm in low-loss skin.

### B. FDTD Modeling

The FDTD method [26] is used to simulate the behavior of the antennas, with and without the breast model present. All FDTD simulations are performed in 3-D, and problem spaces are terminated with perfectly matched layers (PMLs) [27]. Antennas are excited with a differentiated Gaussian pulse of the form

$$V(t) = (t - t_o) e^{(-(t-t_o)^2)/\tau^2} \tag{3}$$

where $\tau = 0.0625$ ns and $t_o = 4\tau$ for a signal with a full-width at half-maximum (FWHM) bandwidth of 5.7 GHz.

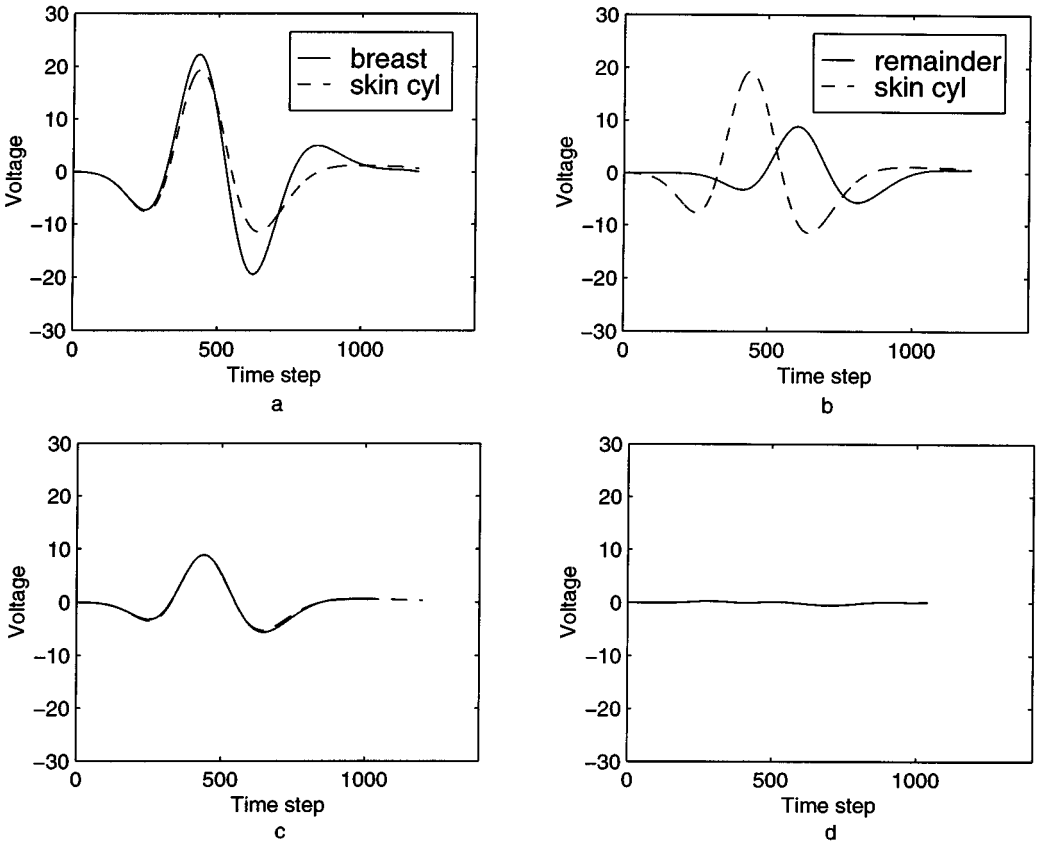


Fig. 2. (a) Returns from breast model and skin cylinder. (b) Remainder after subtraction of signals in (a). (c) Remainder and skin cylinder returns aligned and scaled. (d) Remainder after subtraction of signals in (c).

For antenna characterization, the *LC* computer code[1] is used to model a resistively loaded monopole parallel to the $z$-axis. The antenna is fed by a coax line with 21-$\Omega$ impedance through a hole in the ground plane that is located on the $x$–$y$-plane. A grid size of 0.25 mm is used to discretize the problem space, and PMLs (four or more layers, parabolic profile, 50-dB attenuation) are placed at least 2.25 cm from the antenna. Comparison between simulations with four and six layers showed reflections on the order of 2% of the maximum field value, and an average of 2% difference over the frequency range of 2–8 GHz. For initial antenna characterization, these increased reflections are tolerable in light of decreased computational cost. For four layers of PMLs and 4000 time steps, the CPU time for a simulation is approximately 3.4 h on a four-processor SGI Origin.

With the breast model present, FDTD is used to simulate the operation of a single resistively loaded dipole antenna located 1 or 2 cm from the breast model. Individual simulations are used together to represent an antenna scanned around the model or an array with sequentially excited elements (assuming minimal coupling between elements). Graded meshes are used to increase the resolution close to the antenna (0.25 mm) and in regions of the breast model near the antenna. PMLs (parabolic profile, eight layers, 60-dB attenuation) are placed at a minimum distance of 2 cm from the antennas or breast model. The CPU time for a simulation is 3.5 h on a four-processor SGI Origin.

[1]K. Thomas, *LC User's Guide, Ver. 2.7*, Feb. 1999. [Online.] Available: http://lc.cray.com

### C. Image Formation Algorithms

Several procedures are applied to recorded backscattered signals to form an image of the tumor. The signals are first calibrated, then a skin subtraction algorithm is applied. Finally, all signals are time shifted and added to find the response at a particular point in the domain of interest. An additional image may be formed without skin subtraction in order to define skin boundaries, which are useful in tumor detection.

The antennas are calibrated by subtracting the signal recorded at the antenna without the breast model present. This procedure reduces reflections from PMLs and also reflections inherent in the antenna. Antenna 1 has a half-length of 6.25 mm, which takes about 260 time steps to travel. The breast is 2 cm away, thus, approximately 835 time steps elapse before the first reflection arrives. The signal is transmitted before the first reflection arrives, and reflections from the antenna structure are subtracted out by the calibration procedure.

In the calibrated signal, the reflections from the breast skin are by far of the largest magnitude. If an image is reconstructed without significantly reducing these reflections, then the skin will be well represented, but returns from structures inside of the breast will be obscured. To mitigate the skin returns, an approximation of the skin response is made using reflections from a cylinder of skin (skin phantom). This process is illustrated Fig. 2, which shows the returns from a 6-cm-diameter breast model and a 6-cm-diameter skin cylinder, each located 2 cm from the illuminating antenna. The skin cylinder returns

are subtracted from the breast model returns, and the remainder is shown in Fig. 2(b). The skin cylinder returns are then aligned with and scaled to match the remainder [see Fig. 2(c)]. These signals are subtracted, and the reduced skin response is shown in Fig. 2(d). The effectiveness of the skin subtraction algorithm is assessed by examining the total reduction in skin response, as well as the reduction in the peak-to-peak energy ratio of returns from the tumor to returns from the skin.

In the skin subtraction algorithm, the first step is identifying the portion of the breast reflection that contains the skin returns. The derivative of the breast signal is taken, and is then examined near the peak of the breast signal. The first local minimum to the left-hand side of the peak and the first local maximum to the right-hand side of the peak define the region of interest. The maximum value of the breast signal in the region of interest and the maximum amplitude of the skin cylinder reflection are aligned. The skin cylinder reflection is scaled to the maximum breast signal value, then subtracted from the breast signal over the portion of interest. The resulting signal or remainder is an approximation to the reflection from the inner skin surface. The skin cylinder signal is then aligned with and scaled to fit the remainder. Finally, the first reflection is rescaled to better fit the data. The approximation to the first reflection is used to determine skin location. Skin thickness is estimated from the difference in alignment between the two skin cylinder reflections used to approximate the signal (with an estimate of the electrical properties of skin). For an array of antennas that encircles the breast, the skin subtraction algorithm provides a map of the breast contour. Using information on skin location from the opposite antenna, a time gate may be applied in order to remove reflections from the second skin interface.

After calibration and skin subtraction, correlation detection is applied to the signal to enhance returns. Correlation to the derivative of the excitation signal is selected due to the antenna transfer function.

After calibration, skin subtraction and correlation detection, an image is formed by time shifting and adding the signals to create a synthetic focus [2]. The focus is scanned through the area inside of the array, and each focal point location is assigned to an entry in a matrix. The time delays from each antenna to a particular focal point in the domain are calculated. To points identified as located within the breast, additional time delays are added in order to compensate for travel through the skin. A window corresponding to a maximum of 1 mm and centered on the time delay is identified in each signal, and these contributions are added together. This helps to enhance reflections from structures such as tumors and suppress reflections due to clutter [2]. The signals in the window are summed, and the corresponding matrix entry is assigned this value. The procedure is repeated for each focus point in the domain. Finally, the envelope of the resulting matrix entries is displayed as an image. The quantity displayed is roughly proportional to energy intensity.

Statistical measures are applied to the images in order to quantify improvements realized with variations of the image formation process. Regions of interest (ROI) are defined, and statistics such as sample mean and variance of the pixel values are computed for each ROI. With the assumption of normally distributed pixel values, ROI statistics are compared using Student's t-distribution for the mean and an F-distribution for the variances. ROI are defined for the skin, breast interior, and tumor. The FWHM of the tumor response is defined, and the maximum and mean pixel values as well as the area of the FWHM response are examined.

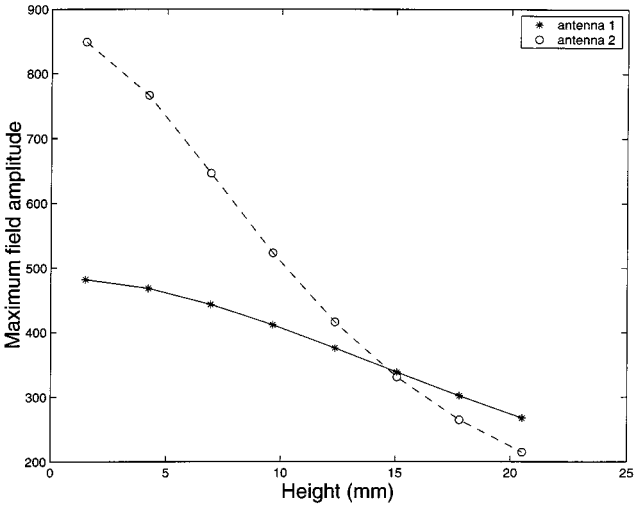


Fig. 3. Variation of maximum field amplitude (in volts per meter) with height above the ground plane at radial distances from antennas 1 and 2 of 2 cm and 1 cm, respectively.

## IV. Results

### A. Antenna Characteristics

For this study, we wish to place the antenna sufficiently far from the breast to reduce coupling, but as close as possible to increase the received returns. The variation in power with distance from antenna 1 has been examined at various heights above the ground plane to determine the far-field distance. For heights equal or less than the antenna length, results indicate that the power distribution at a radial distance of 2 cm from the antenna varies with $1/R^2$ and, thus, the far-field assumption is valid. By extension, the far-field approximation is likely to be valid at 1 cm from antenna 2 in the skin.

The behavior of the fields at the object distance has been investigated by examining field amplitudes, time-domain gain, and fidelity. Fields are examined at heights above the ground plane ranging from 1.375 to 21.625 mm, and at radial distances of 2 and 1 cm from antenna 1 and antenna 2, respectively. Field amplitude variation with distance above the ground plane is shown in Fig. 3 for antennas 1 and 2. For this application, the antenna beamwidth is defined as the FWHM of the energy intensity at the object distance (i.e., planar rather than following the beam intensity pattern). Antenna 2 has both larger field amplitude and smaller beamwidth. Time-domain gain computations (Fig. 4) show a slightly larger maximum gain for antenna 2, as well as variation with height above the ground plane that corresponds to the observed narrower beamwidth. The time signatures of the fields over the beamwidth have also been examined. Both antennas show high fidelity with respect to the first derivative of the excitation pulse, with the fidelity of antenna 1 varying from 0.96 to 0.98, and the fidelity of antenna 2 varying from 0.95 to 0.96 over the beamwidth.

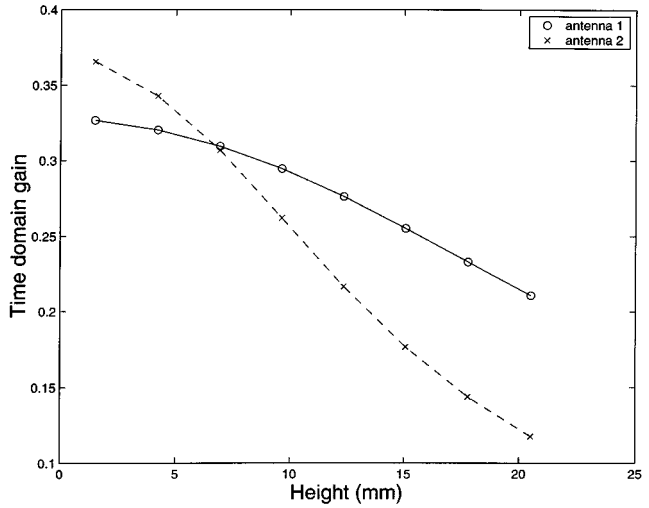


Fig. 4. Time-domain gain computed for various heights above the ground plane for antenna 1 at a radial distance of 2 cm, and antenna 2 at a radial distance of 1 cm.

The frequency responses of the antennas are important for this ultrawide-band application. The transmitting transfer functions for antennas 1 and 2 have been computed using the voltage spectrum of the input to the coax line, as well as the field components at radial distances of 2 cm and 1 cm, respectively. The transfer functions of both antennas confirm that the radiated field is a derivative of the input signal. Antenna 1 has a slightly flatter response over the frequency range, while for antenna 2, the amplitude of the transfer function is greater. The larger amplitude is due to greater field amplitude and better matching of antenna 2 to the input coax line: 18% of the input energy is reflected from antenna 2, while 28% is reflected from antenna 1. To examine the receiving transfer function, two antennas of design 1 are placed 4 cm apart. The incident field is considered to be 2 cm from the receiving antenna and approximated by fields computed with a single antenna, as the second antenna perturbs the fields only slightly. The receiving transfer function is found to be relatively flat over the frequency range, with increasing attenuation at higher frequencies.

The antenna characterization shows that both antennas exhibit ultrawide-band behavior, and that the breast is illuminated with the derivative of the excitation signal. The results also suggest that a greater and more spatially selective response from tumors be expected from antenna 2 (in low-loss skin) due to the greater field amplitude and narrower beamwidth.

### *B. Image Formation*

The effect of the skin subtraction algorithm has been investigated by examining single antenna returns and reconstructed images. A 6-cm-diameter breast model with 2-mm skin thickness and a 6-mm-diameter tumor located at the center is immersed in a low-loss breast-like liquid and illuminated by antenna 1. For the heterogeneous breast model, the antenna is moved to 30 locations that are spaced 1 cm apart on a 10-cm-diameter circle surrounding the breast. The homogeneous breast model is symmetric, thus, the returns at one antenna position are used to represent the returns recorded at the 30 antenna locations examined in the heterogeneous case. First, the skin subtraction algorithm is applied to a single return. For both breast models, the skin response is reduced by an average of 92% by the subtraction algorithm. The peak-to peak energy ratio of returns from the tumor to returns from the skin is increased from $-47.8$ to $-21.8$ dB for the homogeneous breast model, and from $-48$ to $-23.2$ dB for the heterogeneous model. Secondly, images are reconstructed using all 30 returns. Figs. 5 and 6 compare images of the heterogeneous breast model reconstructed with and without skin subtraction. Without skin subtraction (Fig. 5), the skin response is the dominant component of the image. The FWHM response of the skin is about 1 cm, which agrees with the FWHM response observed before time shifting and adding the responses. This response is larger than the physical extent of the skin and, thus, the diameter of the breast tissue cylinder appears smaller than 5.6 cm. The FWHM response of the skin is identified using image thresholding, which zeros pixel values below the half of the maximum pixel value. The maximum extent of the FWHM response of the skin into the breast interior is indicated in Fig. 5 with a black line. The image in Fig. 6 reconstructed with skin subtraction illustrates that the application of this algorithm allows for tumor detection on images. The extent of the skin response into the breast interior observed without skin subtraction is also indicated in Fig. 6 for reference. This aids in tumor detection, as responses outside of this limit are likely due to imperfect skin subtraction and not tumors.

To further evaluate the robustness of the skin subtraction algorithm, it has been applied to various skin thicknesses and shapes. Table I compares estimated skin location, thickness and percent energy remaining in the skin signal for a few test cases, illustrating the robustness of this algorithm.

The skin subtraction algorithm is not easily extended to the case of the antenna in a skin-like substance, as the summed returns from single boundaries with skin and breast tissue phantoms are dissimilar to returns from a thin layer of skin. Evaluation of antenna performance suggests larger tumor returns for antenna 2, and this is verified by reconstructing images with a simple skin subtraction algorithm. This simple algorithm subtracts returns from tumorless breast models from returns recorded for breast models with a tumor. In the images reconstructed for the system immersed in low-loss skin, the ratio between the mean response of the 6-mm tumor and breast interior ROI is 18 : 1. For a similar image reconstructed with the system in breast tissue for comparison, the ratio of the tumor and interior ROI means is only 9 : 1.

### *C. System Evaluation*

To further evaluate features of the proposed system, two investigations have been performed. First, images of the heterogeneous and homogeneous breast models described in the previous section are reconstructed with various numbers of antennas. Statistics for antennas spaced by 1 cm (30 antennas), 2 cm (15), and 1 cm (10) are summarized in Table II. A larger difference between the maximum tumor value and the mean of the interior ROI, plus a smaller standard deviation in the interior ROI indicate improved detection. Second, the response to smaller tumors is investigated. Table III compares statistics for tumors of smaller diameter placed in a homogeneous breast model. The maximum and mean of the tumor response decrease

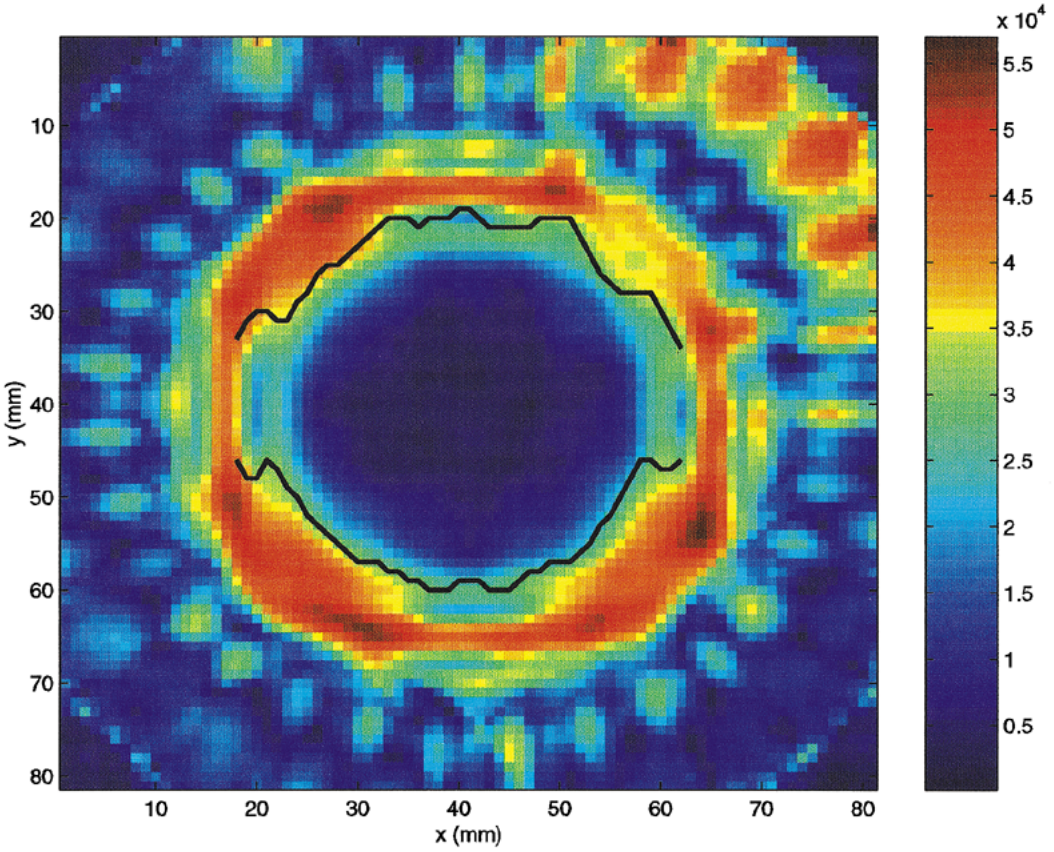


Fig. 5. Image formed without skin subtraction. The breast model is centered at ($x = 40$ mm, $y = 40$ mm), and is 6 cm in diameter. The red portion of the image corresponds to the skin. The line shows the inner skin surface.

as the tumor size decreases, as expected. However even without a tumor present, a significant response is evident at the center of the breast. To gain insight into the cause of this "ghost" tumor, an image of a tumor-free heterogeneous model is also reconstructed. Statistics for and visual inspection of this image do not indicate the presence of a tumor.

## V. Discussion

### A. Antennas

Although the small antennas ($\lambda/2$ in tissue) examined in this paper are capable of detecting tumors, the dynamic range requirements for a practical system are challenging. For a system immersed in low-loss breast tissue, the peak-to-peak energy of returns from a 6-mm-diameter 3-cm-deep tumor are 110 dB below the peak-to-peak energy in the excitation signal. Methods of increasing the level of these returns are required for a practical system to detect smaller tumors. Immersing the system in low-loss skin is one method of increasing the received returns. Characteristics, such as narrower beamwidth and greater field amplitude of the antenna designed for operation in low-loss skin, improve sensitivity to tumors. Images reconstructed with a simplified skin subtraction algorithm confirm this observation. Another method of increasing the recorded tumor response is increasing the length and receiving area of the antenna. For example, Hagness *et al.* reported that returns for a 3-cm-deep tumor of 5.28-mm-diameter were −83 dB below the excitation pulse when illuminated by a resistively loaded bow-tie antenna of 8-cm length [3]. The antenna was located on the skin, whereas the antennas in this paper are located 5 cm from the tumor. Another advantage of longer antennas comes with scanning the array vertically past the breast, as tumors are illuminated from a wider range of antenna locations, and this decreases the possibility of missing a tumor. Thus, further rigorous evaluation of the characteristics of other antennas should lead to selection of optimal antennas for a practical system.

### B. Image Formation

The effectiveness of the skin subtraction algorithm for a breast model immersed in low-loss breast tissue is illustrated by the reduction in skin response, as well as the increase in the relative tumor response by approximately 25 dB. Although the tumor response remains on the order of 20 dB below that of the skin, this provides in the ability to detect tumors, as illustrated by the comparison of Figs. 5 and 6.

Despite its simplicity, the skin subtraction algorithm described in this paper is robust with respect to changes in skin thickness, and size, shape, and position of skin cylinder used in the approximation, as summarized in Table I. Although the skin reflections are reduced less effectively for skin layers less than 2-mm thick, the attenuation of the tumor signal is also reduced. The test cases of overlapping cylinders and the cone indicate that this algorithm will, in principle, work for an unknown breast shape. The results for the heterogeneous breast model

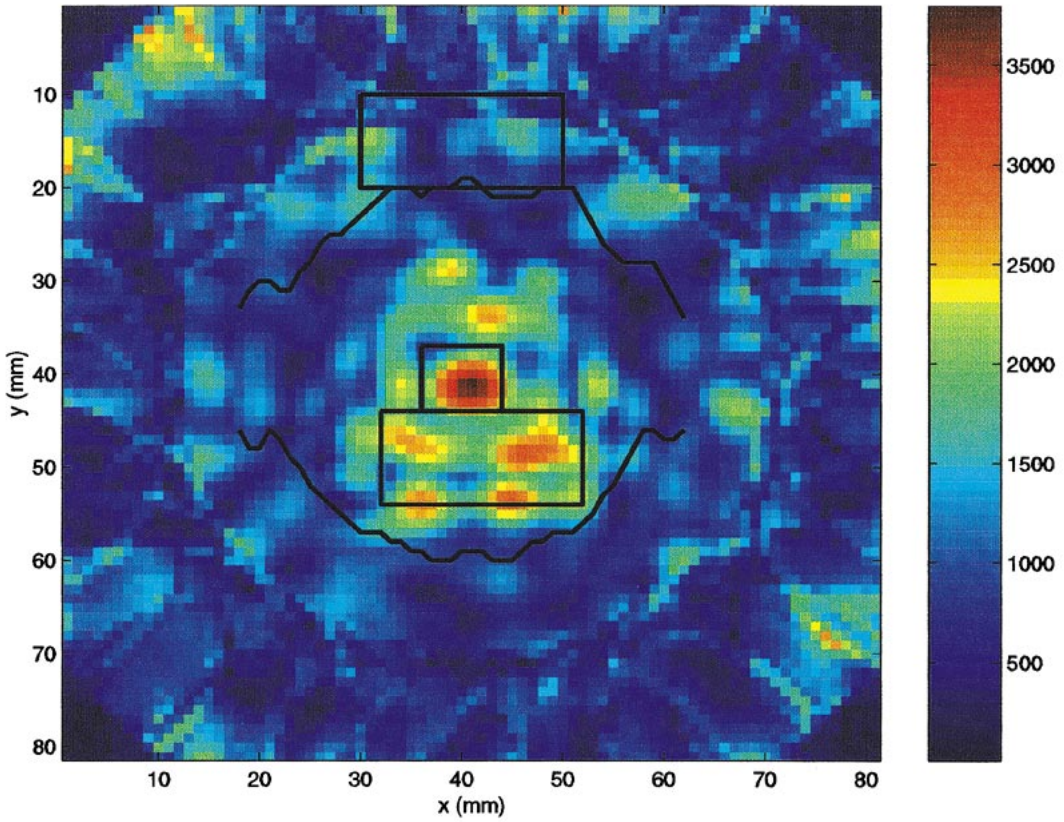


Fig. 6. Image of 6-cm breast model formed after skin subtraction. The tumor is located at ($x = 40$ mm, $y = 40$ mm), and is 6 mm in diameter. The line shows the inner skin surface, and the boxes indicate the ROI for skin, breast interior, and tumor.

TABLE I
PERFORMANCE OF SKIN SUBTRACTION ALGORITHM (VALUES IN BRACKETS GIVE THE NOMINAL DIMENSION). THE HEIGHT OF CYLINDERS IN ROWS 1–4 IS 7 cm, AND THE HEIGHT OF THE CYLINDERS IN ROW 5 IS 4 cm

| Breast Model Diameter (cm) | Skin cylinder Diameter (cm ) | Skin cylinder Distance to antenna (cm) | Location (cm) | Thickness (mm) | Energy Remaining (%) |
|---|---|---|---|---|---|
| 6 | 6 | 2 | 2.24 (2) | 2.1 (2) | 6.3 |
| 6 | 10 | 3 | 2.24 (2) | 1.5 (2) | 18 |
| 2 of 6 (overlapping)  | 6 | 2 | 2.28 (2) | 2 (2) | 11 |
| 6 to 4 (conical) | 6 | 2 | 2.5 (2) | 2 (2) | 5.4 |
| 10 | 10 | 3 | 3.12 (3)<br>3.13 (3.05)<br>3.15 (3.1)<br>3.07 (2.95) | 2.1 (2)<br>2 (1.5)<br>1.9 (1)<br>2.6 (2.5) | 11.8<br>17.4<br>24.1<br>12.3 |

indicate that the algorithm works with small perturbations in the electrical properties of the breast interior. The effectiveness of the algorithm with respect to perturbations in the dielectric properties of skin must be evaluated, as variations in this property from patient to patient are expected. Finally, comparison of results for systems immersed in low-loss breast tissue and skin showed a twofold increase of the tumor response with the latter system. These results were obtained with a simple skin subtraction algorithm, as the algorithm introduced for the low-loss breast tissue is not extensible to low-loss skin. Development of an improved skin subtraction algorithm for this configuration is required in order to realize this improvement in sensitivity to tumors.

### C. System-Performance Evaluation

Two aspects of system performance have been investigated: the influence of the number of antennas on reconstructed images, and the ability to detect smaller tumors. In all of the reconstructed images, tumors are easily detected by visual inspection. Statistics describing changes with increased antenna spacing

TABLE II
STATISTICS COMPUTED FOR ROIS OF VARIOUS IMAGES. MODEL 1 IS A HETEROGENEOUS 6-cm DIAMETER BREAST MODEL OF LENGTH 7 cm AND PLACED 2 cm FROM THE ANTENNAS. MODEL 2 IS A HOMOGENEOUS MODEL OF THE SAME DIMENSIONS. THE BREAST INTERIOR ROI CONTAINS 231 PIXELS

| Model | Antennas | Interior Mean (*1000) | Interior Standard deviation | Tumor Max (*1000) | FWHM Tumor Mean (*1000) | FWHM Tumor Pixels |
|---|---|---|---|---|---|---|
| 1 | 30 | 2.1 | 432 | 3.79 | 2.7 | 56 |
| 1 | 15 | 2.1 | 600 | 4.07 | 2.9 | 52 |
| 1 | 10 | 2.5 | 787 | 4.62 | 3.7 | 44 |
| 2 | 30 | 1.9 | 696 | 5.8 | 4.3 | 47 |
| 2 | 15 | 1.9 | 787 | 6.02 | 4.4 | 46 |
| 2 | 10 | 2.2 | 600 | 5.96 | 4.4 | 47 |

TABLE III
RESPONSE OF TUMORS OF SMALLER SIZES IN IMAGES. BREAST MODELS ARE THE SAME AS IN TABLE II, AND 15 ANTENNAS ARE USED TO RECONSTRUCT IMAGES

| Model | Tumor Diameter (mm) | Interior Mean (*1000) | Tumor Max (*1000) | FWHM Tumor Mean (*1000) | FWHM Tumor Pixels |
|---|---|---|---|---|---|
| 2 | 4 | 1.8 | 4.93 | 3.6 | 49 |
| | 2 | 1.75 | 3.9 | 2.9 | 57 |
| | - | 1.74 | 3.77 | 2.76 | 60 |
| 1 | - | 1.9 | 2.35 | 1.7 | 56 |

from 1 to 3 cm are summarized in Table II for heterogeneous and homogeneous models. For the heterogeneous model, the maximum of the tumor response increases with fewer antennas, however the FWHM tumor area decreases, and the mean and standard deviation of the interior ROI both increase. While these changes are not statistically significant, partly due to the large number of pixels in the interior region, they are visually significant. For the heterogeneous model, the ability to detect tumors appears to decrease with a decreasing number of antennas. Different trends are observed with a homogeneous model, as there is less of a change in the standard deviation and tumor area with fewer antennas. Additionally, the ratios between the means of the FWHM tumor response and interior ROI are much larger than for the heterogeneous model. Finally, the examination of the tumor response with a decrease in tumor size led to discovery of the "ghost" tumor in the homogeneous model. This is not present in heterogeneous model, and is likely due to the use of the same signal to represent returns from different antenna positions. Overall, comparisons between images of homogeneous and heterogeneous breast models indicate that, while homogeneous models are reasonable for initial feasibility testing, heterogeneous models are required for rigorous testing of algorithms and development of 3-D imaging procedures. Further work is needed to determine the minimum tumor sizes at various depths that are detected. Another system parameter that requires evaluation is resolution. That is, the distances between two tumors, a tumor and a blood vessel, and a tumor and the skin that are required to identify two distinct objects must be determined.

Further considerations for a practical system include implementation of the calibration procedure and skin subtraction algorithm, as well as the development of ultrawide-band baluns. Calibration could be performed without the breast present. The calibration procedure would account for small reflections from multilayer microwave absorbers terminating the immersion liquid. Time gating, similar to that in network analyzers, can be used to remove these and antenna reflections in an experimental system. To obtain the reflections from a cylinder of skin used for skin subtraction in a real system, a calibration phantom could be used.

The proposed configuration of our system provides a reference frame for image reconstruction, but is not capable of scanning the upper outer quadrant of the breast where many tumors appear. A practical system may require a hybrid of our configuration and that of Hagness *et al.* or a modification to our system. Another approach is suspending the antennas in a bra filled with lossless material [28]. Although this is a more complicated implementation of the system, this preserves the location of the antennas with respect to each other, and maintains the distance between the antennas and skin.

## VI. CONCLUSIONS

An alternative configuration for confocal microwave imaging of the breast has been evaluated for detection of spherical tumors. In this configuration, an array of antennas encircles the breast, providing a frame of reference for image reconstruction. For the system immersed in a low-loss breast-like liquid, algorithms are developed to deal with the dominant reflections from the skin, resulting in successful detection of tumors. For the system immersed in a low-loss skin-like liquid, initial feasibility studies show increased sensitivity to tumors. However, skin subtraction algorithms require further development. While the small antennas investigated with both systems show the ability to detect tumors, improvements to the antennas are required for a practical system that detects small tumors. Overall, confocal microwave imaging appears to be a feasible approach to breast tumor detection, and extensible to different system configurations.

## ACKNOWLEDGMENT

The authors are grateful to the reviewers of this paper's manuscript for their many helpful comments. The authors would also like to thank Dr. S. Hagness, University of Wisconsin, Madison, for her encouragement and many interesting discussions.

## REFERENCES

[1] P. M. Meaney, K. D. Paulsen, J. T. Chang, M. W. Fanning, and A. Hartov, "Nonactive antenna compensation for fixed-array microwave imaging: Part II—Imaging results," *IEEE Trans. Med. Imag.*, vol. 18, pp. 508–518, June 1999.

[2] S. C. Hagness, A. Taflove, and J. E. Bridges, "Two-dimensional FDTD analysis of a pulsed microwave confocal system for breast cancer detection: fixed-focus and antenna-array sensors," *IEEE Trans. Biomed. Eng.*, vol. 45, pp. 1470–1479, Dec. 1998.

[3] ——, "Three-dimensional FDTD analysis of a pulsed microwave confocal system for breast cancer detection: Design of an antenna-array element," *IEEE Trans. Antennas Propagat.*, pp. 783–791, May 1999.

[4] L. E. Larsen and J. H. Jacobi, Eds., *Medical Applications of Microwave Imaging*. New York: IEEE Press, 1986.

[5] M. Miyakawa, "Tomographic measurement of temperature change in phantoms of the human body by chirp radar-type microwave computed tomography," *Med. Biol. Eng. Comput.*, vol. 31, pp. S31–S36, 1993.

[6] K. D. Paulsen and P. M. Meaney, "Nonactive antenna compensation for fixed-array microwave imaging—Part I: Model development," *IEEE Trans. Med. Imag.*, vol. 18, pp. 496–507, June 1999.

[7] A. Franchois, A. Joisel, C. Pichot, and J.-C. Bolomey, "Quantitative microwave imaging with a 2.45-GHz planar microwave camera," *IEEE Trans. Med. Imag.*, vol. 18, pp. 550–561, Aug. 1998.
[8] A. E. Souvorov, A. E. Bulyshev, S. Y. Semenov, R. H. Svenson, A. G. Nazarov, Y. E. Sizov, and G. P. Tatsis, "Microwave tomography: A two-dimensional Newton iterative scheme," *IEEE Trans. Microwave Theory Tech.*, vol. 46, pp. 1654–1658, Nov. 1998.
[9] W. C. Chew, "Imaging and inverse problems in electromagnetics," in *Advances in Computational Electrodynamics: The Finite-Difference Time-Domain Method*, A. Taflove, Ed. Norwood, MA: Artech House, 1998, ch. 12.
[10] F.-C. Chen and W. C. Chew, "Time-domain ultra-wideband microwave imaging radar system," in *Proc. IEEE Instrum. Meas. Conf.*, 1998, pp. 648–650.
[11] E. C. Fear and M. A. Stuchly, "Microwave system for breast tumor detection," *IEEE Microwave Guided Wave Lett.*, vol. 9, pp. 470–472, Nov. 1999.
[12] E. M. Johansson and J. E. Mast, "Three-dimensional ground penetrating radar imaging using synthetic aperture time-domain focusing," *Proc. SPIE*, vol. 2275, pp. 205–214, 1994.
[13] J. I. Halman, K. A. Shubert, and G. T. Ruck, "SAR processing of ground-penetrating radar data for buried UXO detection: Results from a surface-based system," *IEEE Trans. Antennas Propagat.*, vol. 46, pp. 1023–1027, July 1998.
[14] S. Gabriel, R. W. Lau, and C. Gabriel, "The dielectric properties of biological tissues: II. Measurements in the frequency range 10 Hz to 20 GHz," *Phys. Med. Biol.*, vol. 41, pp. 2251–2269, 1996.
[15] S. C. Hagness, A. Taflove, and J. E. Bridges, "Wideband ultralow reverberation antenna for biological sensing," *Electron. Lett.*, vol. 33, no. 19, pp. 1594–1595, Sept. 1997.
[16] J. Maloney and G. Smith, "A study of transient radiation from the Wu–King monopole—FDTD analysis and experimental measurements," *IEEE Trans. Antennas Propagat.*, vol. 41, pp. 668–676, May 1993.
[17] T. Montoya and G. Smith, "A study of pulse radiation from several broad-band loaded monopoles," *IEEE Trans. Antennas Propagat.*, vol. 44, pp. 1172–1182, Aug. 1996.
[18] T. Montoya and G. Smith, "Vee dipoles with resistive loading for short-pulse ground-penetrating radar," *Microwave Opt. Technol. Lett.*, vol. 13, pp. 132–137, Oct. 1996.
[19] T. T. Wu and R. W. P. King, "The cylindrical antenna with nonreflective resistive loading," *IEEE Trans. Antennas Propagat.*, vol. 13, pp. 369–373, May 1965.
[20] L. C. Shen and R. W. P. King, "Corrections to 'The cylindrical antenna with nonreflective resistive loading'," *IEEE Trans. Antennas Propagat.*, vol. AP-13, p. 998, Nov. 1965.
[21] M. Kanda, "Time domain sensors for radiated impulsive measurements," *IEEE Trans. Antennas Propagat.*, vol. 31, pp. 438–444, May 1983.
[22] K. Esselle and S. S. Stuchly, "Pulse receiving characteristics of resistively loaded dipole antennas," *IEEE Trans. Antennas Propagat.*, vol. 38, pp. 1677–1683, Oct. 1990.
[23] D. Lamensdorf and L. Susman, "Broadband-pulse-antenna techniques," *IEEE Antennas Propagat. Mag.*, vol. 36, pp. 20–30, Feb. 1994.
[24] J. D. Taylor, Ed., *Introduction to Ultra-Wideband Radar Systems*. Boca Raton, FL: CRC Press, 1995.
[25] O. E. Allen, D. A. Hill, and A. R. Ondrejka, "Time-domain antenna characterizations," *IEEE Trans. Electromag. Compat.*, vol. 35, pp. 339–345, Aug. 1993.
[26] K. Umashankar and A. Taflove, *Computational Electromagnetics*. Norwood, MA: Artech House, 1993.
[27] J. Berenger, "A perfectly matched layer for the absorption of electromagentic waves," *J. Comput. Phys.*, vol. 114, pp. 185–200, 1994.
[28] E. Okoniewska, private communication, July 1999.

**E. C. Fear** (S'98) received the B.A.Sc. degree in systems design engineering from the University of Waterloo, Waterloo, ON, Canada, in 1995, the M.A.Sc. degree in electrical engineering from the University of Victoria, Victoria, BC, Canada, in 1997, and is currently working toward the Ph.D. degree in electrical engineering at the University of Victoria.

Her research interests involve the interaction of electromagnetic fields with living systems, including the interaction of low-frequency fields with biological cells and microwave breast cancer detection.

Ms. Fear is the student representative of the IEEE Engineering in Medicine and Biology Society (IEEE EMBS) Administrative Committee. She was the recipient of the Whitaker Foundation Student Paper Contest Award presented at the 19th Annual International Conference of the IEEE EMBS.

**M. A. Stuchly** (S'71–SM'76–F'91) received the M.Sc. degree in electrical engineering from the Warsaw Technical University, Warsaw, Poland, in 1962, and the Ph.D. degree in electrical engineering from the Polish Academy of Sciences, Warsaw, Poland, in 1970.

From 1962 to 1970, she was with the Warsaw Technical University and the Polish Academy of Sciences. In 1970, she joined the University of Manitoba. In 1976, she joined the Bureau of Radiation and Medical Devices in Health and Welfare, Canada, as a Research Scientist. In 1978, she was associated with the Electrical Engineering Department, University of Ottawa, as an Adjunct Professor. From 1990 to 1991, she was a Funding Director of the Institute of Medical Engineering. In 1992, she joined the University of Victoria, Victoria, BC, Canada, as a Visiting Professor with the Department of Electrical and Computer Engineering. Since January 1994, she has been a Professor and Industrial Research Chairholder funded by the National Sciences and Engineering Research Council of Canada, BC Hydro, and Trans Alta Utilities. Her current research interests are in numerical modeling of interaction of electromagnetic fields with the human body and wireless communication antennas.